J Electr Eng Technol.2017; 12(?): 1921-718
http://doi.org/10.???/JEET.2017.12.3.1921

ISSN(Print) 1975-0102
ISSN(Online) 2093-7423

Corona Discharge Characteristics and Particle Losses in a Unipolar Corona-needle Charger Obtained through Numerical and Experimental Studies

Panich Intra†, Artit Yawootti* and Phadungsak Rattanadecho**

Abstract – In this paper, the unipolar corona-needle charger was developed and its capabilities were both numerically and experimentally investigated. The experimental corona discharges and particle losses in the charger were obtained at different corona voltage, aerosol flow rate and particle diameter for positive and negative coronas. Inside the charger, the electric field and charge distribution and the transport behavior of the charged particle were predicted by a numerical simulation. The experimental results yielded the highest ion number concentrations of about 1.087×10^{15} ions/m^3 for a positive corona voltage of about 3.2 kV, and 1.247×10^{16} ions/m^3 for a negative corona voltage of about 2.9 kV, and the highest $N_i t$ product for positive and negative coronas was found to about 7.53×10^{13} and 8.65×10^{14} ions/m^3 s was occurred at the positive and negative corona voltages of about 3.2 and 2.9 kV, respectively, and the flow rate of 0.3 L/min. The highest diffusion loss was found to occur at particles with diameter of 30 nm to be about 62.50 and 19.33 % for the aerosol flow rate of 0.3 and 1.5 L/min, respectively, and the highest electrostatic loss was found to occur at particles with diameters of 75 and 50 nm to be about 86.29 and 72.92 % for positive and negative corona voltages of about 2.9 and 2.5 kV, respectively. The numerical results for the electric field distribution and the charged particles migration inside the charger were used to guide the description of the electric field and the behavior of charged particle trajectories to improve the design and refinement of a unipolar corona-needle charger that otherwise could not be seen from the experimental data.

Keywords: Corona discharge, Particle charging, Aerosol charger, Numerical simulation

1. Introduction

Corona discharges are relatively low power partial electrical discharges that develop in zones of highly concentrated electric fields such as at small diameter wires, needles, or sharp edges on the electrode at or near atmospheric pressure [1]. The corona discharge has been applied severally as an electrostatic precipitator, in electrostatic printing and deposition, in ozone production, ionization counting and particle charging [2]. The particle charging application of corona discharging has been successful in its capability to provide high ion concentrations. There have been numerous studied in the past [3]. The literature describes applications for both corona-wire and corona-needle chargers [4].

A corona-needle discharge is widely used as a particle charger because of its simplicity and ability to provide stable and high concentrations of ion without a sheath of air [5-10]. The studies have contributed to the improved performance of these chargers by reducing particle losses inside the charger: (i) the introduction of surrounding sheath air flows at the boundary between the aerosol stream and the wall to allow more space for the charged particles to follow random paths without precipitating on the charger walls [11], (ii) the use of a turbulent jet of unipolar ions in a mixing chamber [12], and (iii) application of an AC or square wave voltage to the electrode instead of DC voltage [13]. In our previous work [14, 15], a simple corona-needle particle charger without sheath air was designed and its electrostatic characteristics were evaluated. It was capable of high concentration and high penetration of unipolar ions for electrostatic discharge and aerosol charging. In this work, the highest ion concentrations in the discharge zone of the charger were found to be 1.71×10^{14} and 5.09×10^{14} ions/m^3 for positive and negative coronas, respectively. At the outlet of the charger, it was found that the highest ion concentration was about 1.95×10^{13}, and 1.91×10^{13} ions/m^3 for positive and negative coronas, respectively. The highest ion penetrations for positive and negative coronas through the charger were 98 %, and 33 %, respectively. However, the corona discharge used in this charger has poor charging

† Corresponding Author: Research Unit of Applied Electric Field in Engineering (RUEE), College of Integrated Science and Technology, Rajamangala University of Technology Lanna, Thailand. (panich_intra@yahoo.com)
* Research Unit of Applied Electric Field in Engineering (RUEE), College of Integrated Science and Technology, Rajamangala University of Technology Lanna, Thailand. (yartit@rmutl.ac.th)
** Center of Excellence in Electromagnetic Energy Utilization in Engineering (CEEE), Department of Mechanical Engineering, Faculty of Engineering, Thammasat University, Thailand. (ratphadu@engr.tu.ac.th)
Received: September 6, 2016; Accepted: June 10, 2017

efficiencies in the ultrafine particle (less than 200 nm) due to high particle losses by the high electric field in the discharge zone of the charger and high particle loss due to diffusion and electrostatic effects during aerosol transport in the charger. The corona discharge in the charger also depended on the polarity of the electrical field and the geometrical configuration of the electrodes of the charger. Depending on the arrangement of major geometrical features inside the corona-needle charger, the important factors influencing on the corona discharge characterizations and particle losses inside the charger has been well known as the electric field distribution of the charger, and the particle transport inside the charger. As the geometry is very complex, it is difficult to carry out detailed and reliable measurements of the electric field distribution, the particle transport in the charger from the experimental study. Numerical simulation provides an alternative approach, which is more reliable and less expensive to guide in describing the electric field distribution and the particle transport behaviors inside the charger that cannot be seen from experiments.

Therefore, the unipolar corona-needle charger was studied quantitatively. The charger's corona discharges and particle losses were numerically and experimentally studied and these were characterized and are discussed at different corona voltage, aerosol flow rate and particle diameter for positive and negative coronas. A numerical model was also developed to study the electric field and charge distribution and the transport behaviors of the charged particles inside this charger that cannot be seen from the experimental data to better understand the charger operation. This provided predictions for the electrical field distribution and the current density in the discharge zone of the charger, the behavior of the charged particle trajectories in the discharge zone of the charger.

2. Materials and methods

2.1 Description of the corona-needle particle charger

Fig. 1 shows the schematic diagram of the modified corona-needle particle charger originally developed by Intra and Tippayawong [14, 15]. The present charger consists essentially of a coaxial needle electrode placed along the axis of a cylindrical tube with a tapered end, and divided into three sections from the top to the bottom in the drawing. The first section (PTFE insulator) was made of a polytetrafluoroethylene (PTFE), and the second (aerosol flow guide) and third (outer electrode) sections were made of stainless steel. The PTFE insulator was an electrical isolator between corona-needle electrode and aerosol flow guide and outer electrode. The PTFE insulator served to hold the corona-needle electrode coaxial with the outer electrode. The corona-needle electrode could be screwed into the PTFE insulator to connect it to either positive or

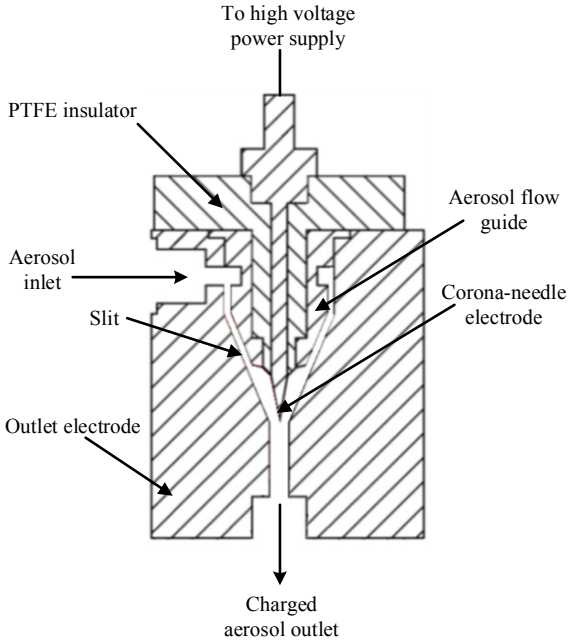

Fig. 1 Schematic diagram of the corona-needle charger

negative DC high voltage supply, typically in the range between 2.7 – 3.0 kV, while the outer electrode was grounded. The needle electrode was made of a stainless steel rod, 3 mm in diameter, ending in a sharp tip. The needle electrode was polished to an extremely fine surface finish to avoid undesirable electric field effects on particle motion due to non-uniform electric field resulting from small surface scratches and imperfections. The needle cone angle was about 10^{o}. The diameter of the outer electrode was 20 mm, its length 20 mm with a conical shape. The orifice diameter was 3.5 mm. The distance between the needle electrode and the cone apex was 1.75 mm. The aerosol flow, typically in the range from 1-5 L/min, was introduced into the charger from the top. In order to avoid particle loss during aerosol transport in the charger due to diffusional, inertial, and electrostatic losses, the conductive aerosol flow guide was used and short residence was maintained in this study. The aerosol flow guide was made of stainless steel which prevents localized build-up of charges on the wall of the charger. The aerosol flow was quickly introduced through an annular slit of 1 mm gap before the discharge zone by the aerosol flow guide.

2.2 Numerical simulation

Three partial differential equations (PDE) were selected and coupled in the commercial software package COMSOL Multiphysics^{TM}, namely, the Poisson's and Navier-Stokes equations as well as the Khan and Richardson force to the accurate model of the corona-needle charger [16]. The computational domain for flow and electric fields of the present charger is shown in Fig. 2. Using the electrostatic module and the PDE module were solved to obtain a

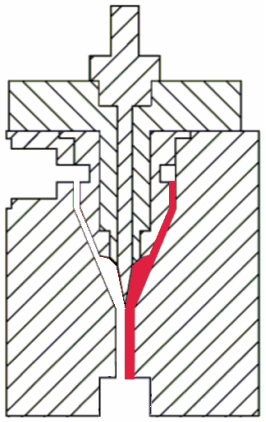

(a) Whole charger

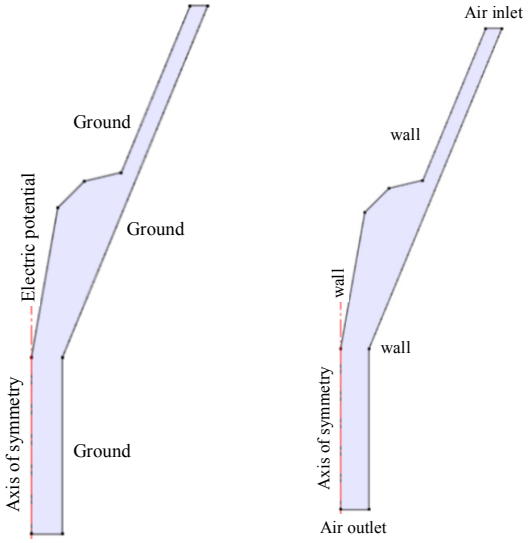

(b) Electric field (c) Flow field

Fig. 2 Computational domain for flow and electric fields of the corona-needle charger

steady state electric potential, electric field and current density. Dirichlet boundary conditions were used in the PDE module, with zero space charge density on the corona-needle electrode boundary along with zero ion concentration on the aerosol flow guide and the outer electrode. In the electrostatic module, a ground (0 V) was implemented on the aerosol flow guide and the outer electrode. Constant electrical potentials were applied to the corona-needle electrode (3 kV). The zero-charge symmetry boundary condition was applied to the boundaries without walls, as given by where is the outward normal from medium and is the electric flux density. In this simulation it could be assumed that no heat transfer occurred in the charger. The flow inside the charger could be assumed to be steady, incompressible and laminar. Based on the principle of momentum conservation, the incompressible Navier-Stokes equations could be applied in this case. A wall boundary condition was implemented on both

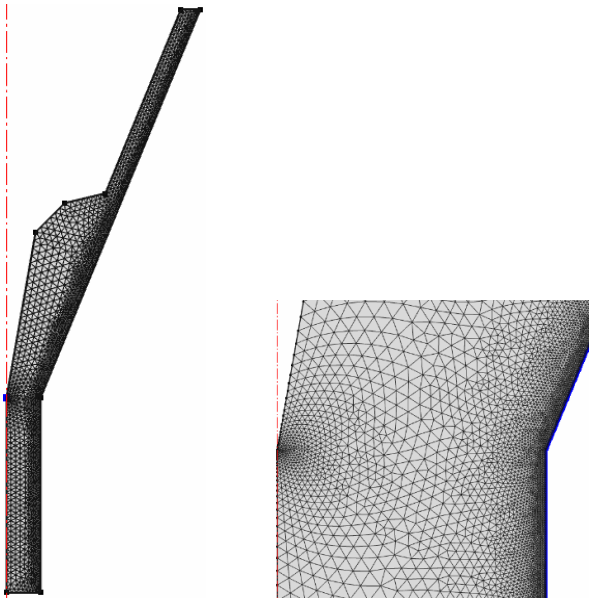

(a) Whole domain (b) Around corona-needle electrode head

Fig. 3 Mesh distribution for flow and electric fields of the corona-needle charger

electrodes, i.e., a pressure of 1.01×10^5 Pa on the outlet and a normal velocity field in the inlet. The operating gas was ambient air (density was 1.19 kg/m^3, viscosity was 1.79×10^{-5} kg/m/s, and the relative permittivity constant was 1.00054). The PTFE insulator permittivity constant was 2.1.

In this study, charged particles with diameters of 30, 50, 75, 100, 150 and 200 nm corresponding to particle masses of 6×10^{-16}, 3×10^{-15}, 6×10^{-15}, 9×10^{-15}, 1×10^{-14} and 2×10^{-14} g, respectively, were used to study the behavior of the charged particle trajectories in the charger. The mean of charge per particle was approximated by White's charging equation for field and diffusion charging [17, 18]. Therefore, the mean of charge per particle was 3.46, 6.21, 9.86, 13.65, 21.54 and 29.73 electrons for the charged particles with diameters of 30, 50, 75, 100, 150 and 200 nm, respectively, at the $N_i t$ product of 2.95×10^{13} ions/m^3 s, the corona voltage of 3 kV, the electric field strength of 4.27×10^4 V/m, and the dielectric constant of 3.0, respectively. Fig. 3 shows the mesh distribution for the flow and electric fields of the charger. The considered problem was discretized with the finite element method (FEM), and triangular elements for the axis-symmetric two-dimensional model were utilized. The mesh was automatically generated by COMSOL [10] and was refined in the critical regions such as the corona-needle electrode head and between outer electrode and insulators. Fig. 4 shows the convergence test results in number of triangular elements of approximately 82,273. The computations were carried out on a desktop running a 64 bit OS Windows 7 Core i5 processors (each 2.40 GHz) and 4 GB of RAM are allowed for solving the model within 5 minutes of computation time. The values of the various parameters used in this

study, are given in Table 1.

2.3 Experimental setup

The experimental setup for investigating the corona discharges and particle losses in a corona-needle charger is shown in Fig. 5. It consisted of a corona-needle charger, an adjustable DC high voltage power supply, a Faraday cup, an electrometer, a high efficiency particulate-free air (HEPA) filter, an atomizer aerosol generator, a dilution chamber, a diffusion dryer, a charged particle removal, an electrostatic classifiers, an ultrafine condensation particle counter and a vacuum pump. The positive and negative high voltage differences on the corona-needle electrode of the charger were applied by an adjustable commercial DC high voltage power supply (model 521721, Leybold Didactic, GmbH, Germany), in the range between 0 and 3.2 kV with a maximum load current of 0.5 mA. The discharge currents in the discharge zone of the charger were directly measured by the electrometer (model 6517A, Keithley Instruments, Inc., Cleveland, OH, USA). The ion number concentration, n_i (ions/m^3) as a function of the discharge current of the charger can be estimated by:

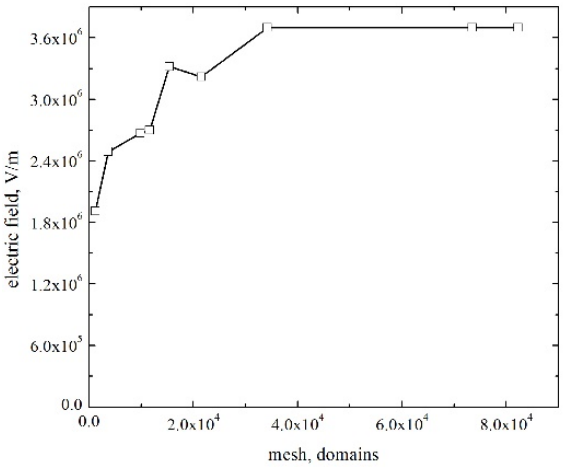

Fig. 4 Grid convergence curve of the model

Table 1. Ranges and values of variables investigated.

Variable	Range
Corona voltage	0 – 3.2 kV
Ion generated	Positive ion (+), Negative ion (–)
Ionized gas	Air
Particle size range	30, 50, 75, 100, 150 and 200 nm
Relative humidity	~ 60 % RH
Flow rate	0.3 and 1.5 L/min
Temperature	~ 30ºC
Pressure	101.3 kPa

$$n_i = \frac{i_i}{eZ_i EA} \tag{1}$$

where i_i is the discharge current of the charger, e is the elementary charge (1.61 × 10^{-19} C), Z_i is the electrical mobility of ions, E is the electric field inside the charger, and A is the inner surface area of the outer electrode where the discharge current is collected.

In order to determine the particle losses in the charger, a NaCl polydisperse aerosol was produced by spraying a NaCl solution with an atomizer aerosol generator (model ATM 226, TOPAS GmbH, Dresden, Germany) and dried to relative humidity less than 30 % RH in a diffusion dryer (model DDU 570, TOPAS, GmbH, Germany) before being introduced into the dilution chamber, where they mixed with clean dilution air via a HEPA capsule filter (model 12-144, Pall Corporation, NY, USA) with filtration efficiency of 99.97 % and retention of 0.3 µm for air/gas. The dilution air flow rate was about 200 m^3/hr. Particles were then classified according to their electrical mobility using an advanced aerosol neutralizer (model 3088, TSI, Inc., Shoreview, MN, USA) and an electrostatic classifier (EC,

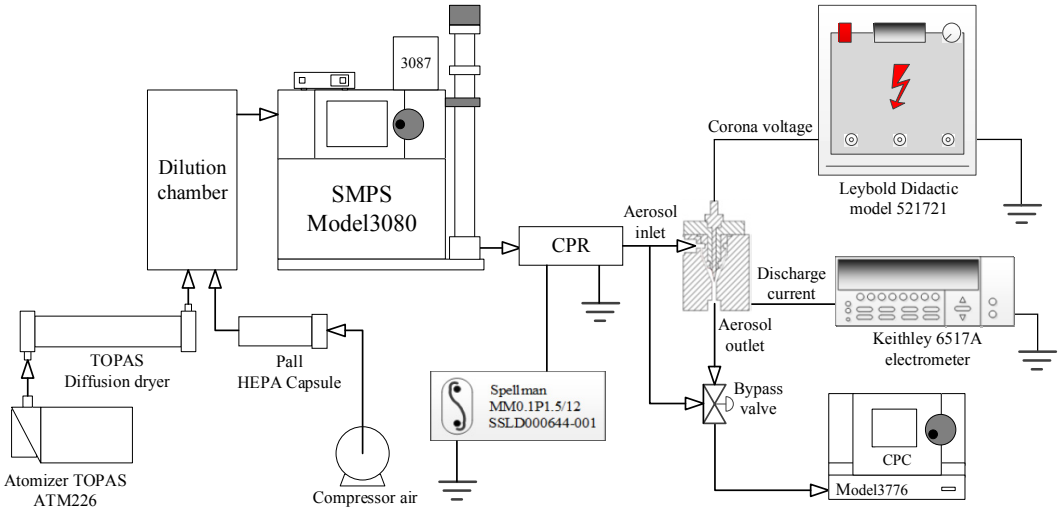

Fig. 5 Experimental setup for investigating the corona discharges and particle losses in the present charger

model 3080, TSI, Inc., Shoreview, MN, USA) with a long-differential mobility analyzer (long DMA, model 3081, TSI, Inc., Shoreview, MN, USA) allowing mobility diameter selection of monodisperse test particles from 30 to 200 nm. Singly charged monodisperse particles were then neutralized and passed through an electrostatic precipitator (CPR) to remove all charged particles, allowing only uncharged particles to enter the charger. After the charged aerosol flow exited the charger, it passed through an ultrafine condensation particle counter (UCPC, model 3776, TSI, Inc., Shoreview, MN, USA). For the particle losses experiments the UCPC was used to measure the particle number concentration upstream and downstream of the charger. Particle losses were measured at the aerosol flow rates between 0.3 and 1.5 L/min. The particle electrostatic loss, L_{el}, and diffusion loss, L_d, inside the charger can be calculated as:

$$L_{el} = \frac{C_{out,OFF} - C_{out,ON}}{C_{in}} \quad (2)$$

$$L_d = \frac{C_{out,OFF}}{C_{in}} \quad (3)$$

where C_{in} is the particle number concentration measured upstream of the charger, $C_{out,OFF}$ is the particle number concentration measured downstream of the charger when no voltage is applied on the charger, and $C_{out,ON}$ is the particle number concentration measured downstream of the charger when the charger is on.

3. Results and Discussion

Fig. 6 shows the numerical calculation of the streamline flow patterns inside the charger at different air flow rates of 0.3 and 1.5 L/min, respectively. Uniform distributions of streamline flow patterns were observed for all flow rates. The highest flow velocities were found to be 0.52 and 2.60 m/s for air flow rates of 0.3 and 1.5 L/min, in the annular slit and in the regions close to the needle trip. Fig. 7 shows the numerical calculation of the electric field, the electric potential and the current density inside the charger. Uniform distributions of electric field, the electric potential and the current density were observed in the discharge zone of the charger. The regions of high towards low intensity are indicated by black, brown, green to white, respectively. As expected, the electric field gradients are increase in an orderly manner. Its gradient was more profound at locations near to the corona-needle electrode. It should be noted that the corona discharge was generally produced by a non-uniform electrostatic field such as that between a wire/needle and plate or a concentric wire and a tube. When the electric field strength was high, air and other gases could undergo electrical breakdown. The only place this breakdown could occur was in the very thin layer

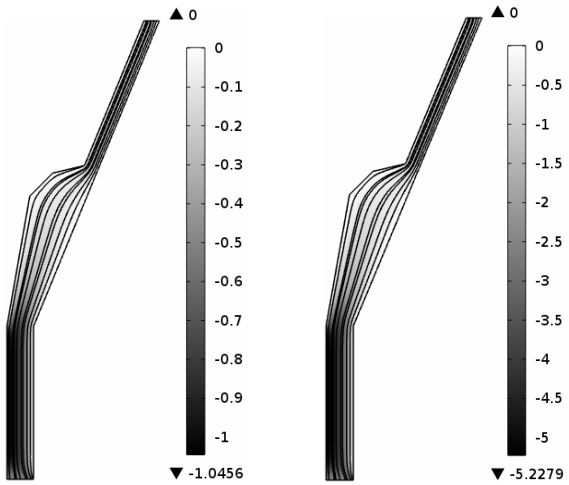

(a) 0.3 L/min (b) 1.5 L/min

Fig. 6 Numerical calculation of the flow field inside the charger

at the needle surface for the case of the needle and the tube. The electrons had sufficient energy to knock off an electron from a gas molecule to create a positive ion and free electrons in this corona discharge zone.

As shown in Fig. 7, the highest electric field and charge density in the discharge zone of the charger were 2.079×10^8 V/m and 25.57×10^{-7} A/m^3, respectively, at a corona voltage of 3.2 kV.

Fig. 8 shows the numerical calculation of the trajectories of charged particles with diameters of 30, 50, 75, 100, 150 and 200 nm inside the charger when no voltage was applied on the charger, at corona voltage of 0 kV and aerosol flow rates between 0.3 and 1.5 L/min. For each aerosol flow rate, it was observed that charged particles with diameter of 30, 50, 75, 100, 150 and 200 nm could pass smoothly through the charger without precipitating on the outer electrode of the charger. Fig. 9 shows the numerical calculation of the trajectories of charged particles with diameters of 30, 50, 75, 100, 150 and 200 nm inside the charger when the charger was on, at corona voltage of 3 kV and aerosol flow rates between 0.3 and 1.5 L/min. At aerosol flow rate of 0.3 L/min, it can be observed that charged particles with diameter smaller than 100 nm slightly precipitated on the outer electrode of the charger, while all of the charged particles could pass smoothly through the charger without precipitating on the outer electrode of the charger for aerosol flow rate of 1.5 L/min. It is well known that the penetration efficiency of charged particles mainly depends on the electric field strength inside the charger and the electrical mobility of particles as a function of a particle diameter. Large particle diameter have higher mean charge than small particle diameter, therefore, the electrostatic force applied on the particle increased with respect to the mean charge per particle as a function of its diameter. An increase in electrostatic force on the charged particles produced a

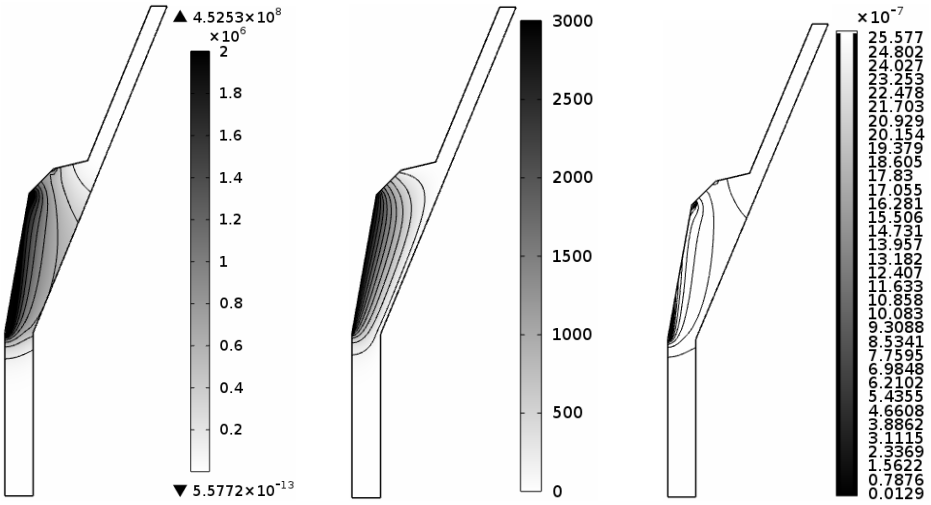

(a) Electric field (b) Electric potential (c) Current density

Fig. 7. Numerical calculation of the electric field, the electric potential and the current density inside the charger

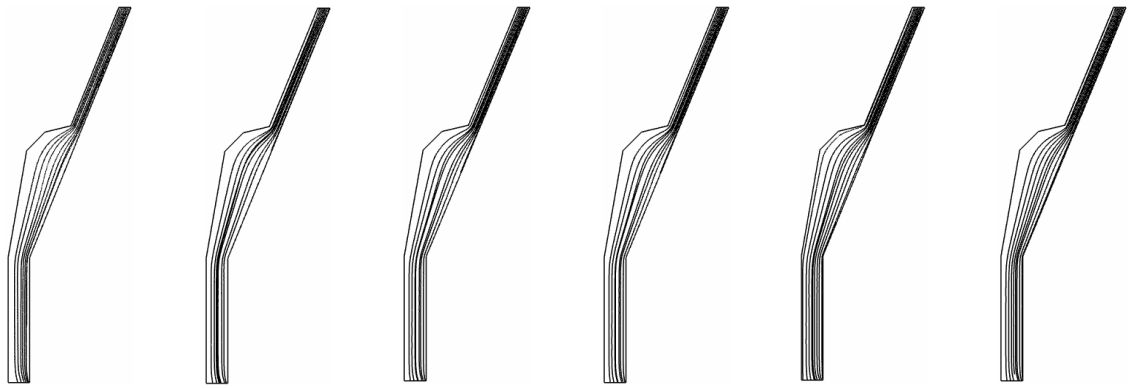

(a) 0.3 L/min

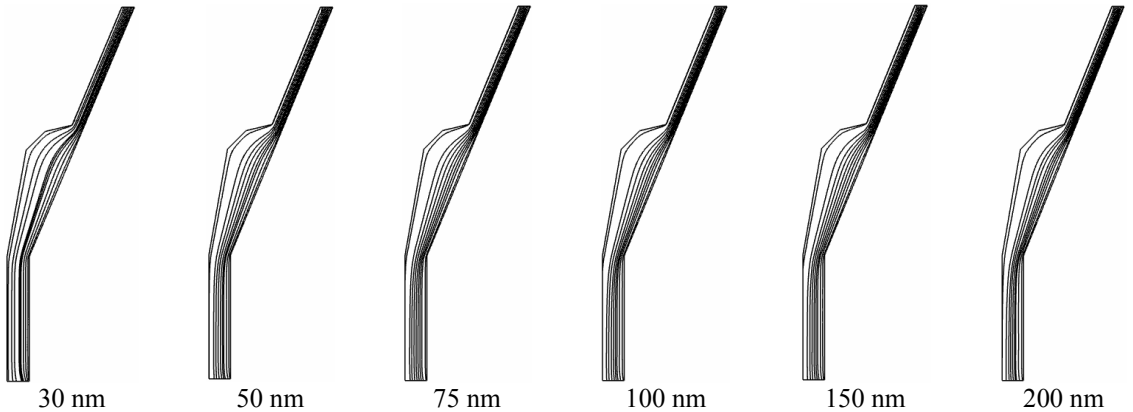

(b) 1.5 L/min

Fig. 8 Numerical calculation of the trajectories of charged particle inside the charger at corona voltage of 0 kV

decrease in the penetration efficiency of the charged particles in the charger. These calculation results can be used to support the improvement of further modification and refinement of the charger and also to understand the mechanisms of the charged particle transport inside the charger.

Fig. 10 shows the variations in discharge current with corona voltage of the charger for positive and negative

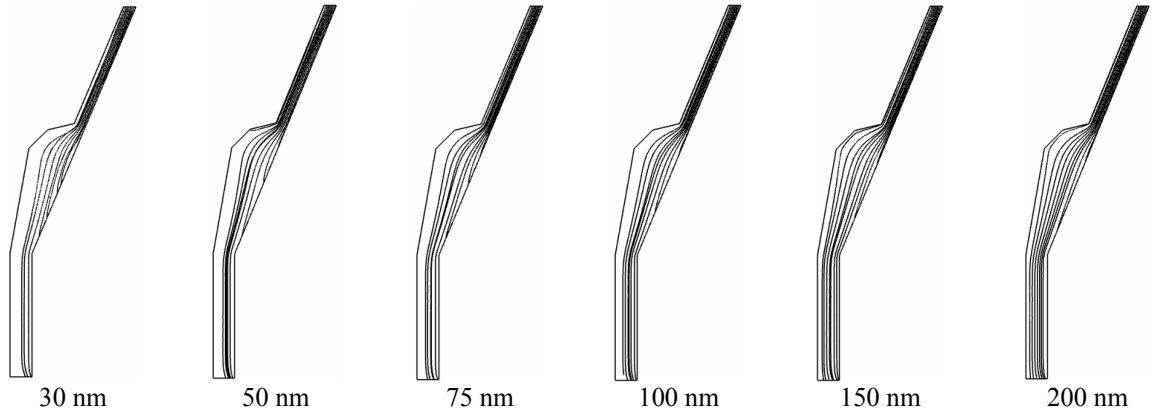

(a) 0.3 L/min

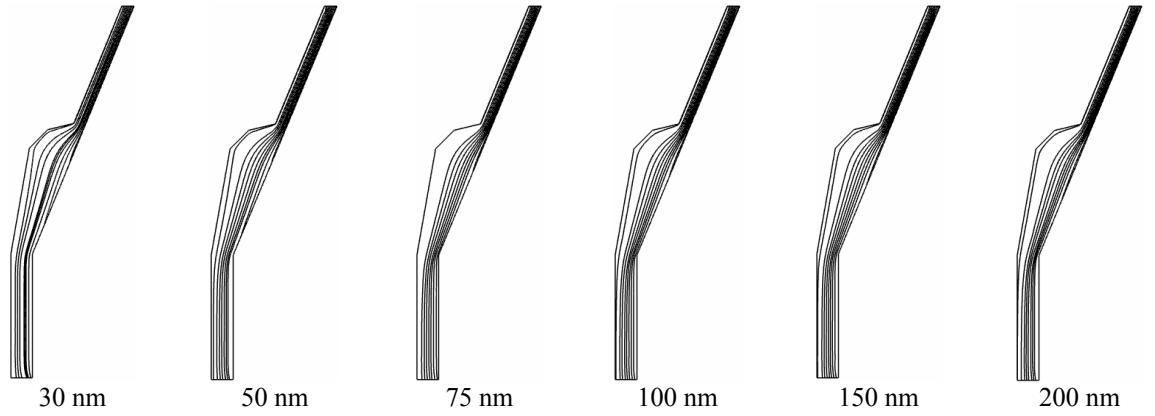

(b) 1.5 L/min

Fig. 9 Numerical calculation of the trajectories of charged particle inside the charger at corona voltage of 3 kV

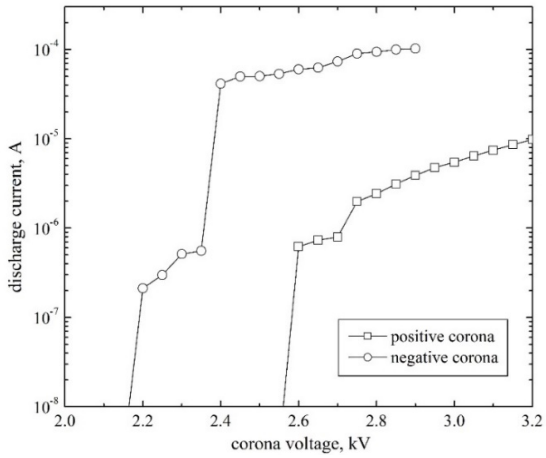

Fig. 10. Variations in discharge current with corona voltage of the charger for positive and negative coronas

coronas. Both positive and negative corona voltages were varied from 0 to 3.2 kV at an operating pressure of about 101.3 kPa. It was found that both positive and negative discharge currents increased monotonically with an increase in the corona voltage. The corona onset voltages were 2.6 and 2.2 kV for positive and negative ions, respectively. As shown in the plot, the spark-over phenomenon occurred for the positive corona at voltages larger than 3.2 kV and for a negative corona at voltages larger than 2.9 kV. It should be noted that the corona discharge started with a burst pulse corona and proceed to a streamer corona, glow corona, and spark discharge as the applied voltage increased for a positive corona in the needle-plate electrode configuration. For a negative corona in the same geometry, the initial form of discharge would be the Trichel pulse corona, followed by the pulse less corona and spark discharge as the applied voltage increases [1]. At the same voltage, the discharge currents for negative ions were slightly higher than those for positive ions. This was expected because negative ions have higher electrical mobility than positive ions. Therefore, negative ions were more likely to impact and deposit on the outer electrode wall of the charger due to the electrostatic force [19].

Fig. 11 shows the variations in ion number concentration with corona voltage in the discharge zone of the charger for positive and negative coronas. The mean number concentration of ions in the discharge zone of the charger was calculated by Eq. (1). The increase of the ion number concentration depended on the corona voltage. In a range

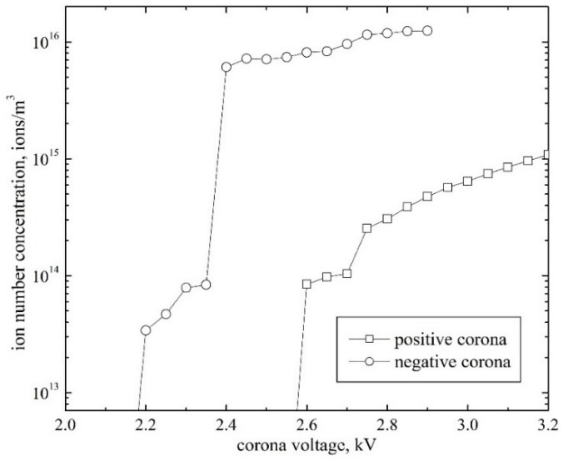

Fig. 11. Variations in ion number concentration with corona voltage of the charger for positive and negative coronas

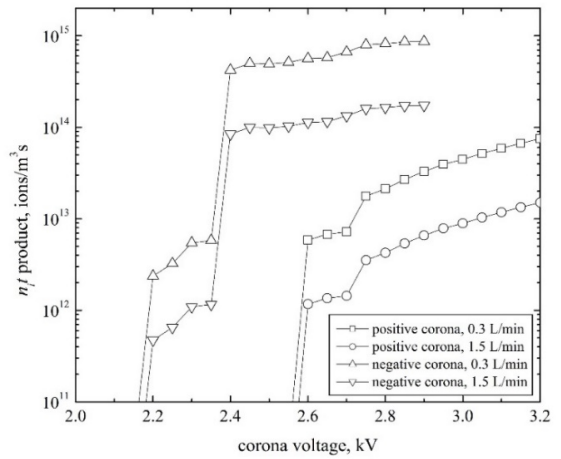

Fig. 12. Variations in N_it product with corona voltage of the charger at different aerosol flow rates for positive and negative coronas

well above the corona onset voltage, it is generally known that the number concentration of a negative ion is larger than the corresponding for a positive ion. The highest ion number concentrations in the discharge zone of the charger were 1.087×10^{15} for a positive corona voltage of about 3.2 kV, and 1.247×10^{16} ions/m^3 for negative corona voltages of about 2.9 kV. It was observed that the magnitudes of the discharge current and the ion number concentration for positive and negative coronas in the discharge zone of this charger were approximately 8 and 2 times higher than those from the Intra and Tippayawong charger [9] at corona voltages of about 3.0 and 2.6 kV, an air flow rate of about 5 L/min for positive and negative coronas, respectively. Fig. 12 shows the variations in N_it product with corona voltage in the discharge zone of the charger at different aerosol flow rates for positive and negative coronas. In this study, the charging times were found to be

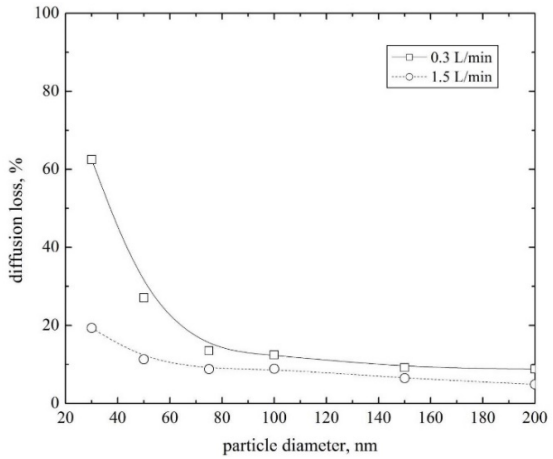

Fig. 13 Variations in diffusion loss with particle diameter of the charger at different aerosol flow rate

about 0.07 and 0.014 sec for the flow rates of about 0.3 and 1.5 L/min, respectively. It was shown that the N_it product decreased with increasing flow rate because higher flow rate or shorter residence time lowered the N_it product. Increases in corona voltage produced a monotonic increase in ion number concentration, hence the N_it product. It was also shown that the highest N_it product for positive and negative coronas was found to be about 7.53×10^{13} and 8.65×10^{14} ions/m^3 s occurring at the positive and negative corona voltages of about 3.2 and 2.9 kV, respectively, at the flow rate of 0.3 L/min.

Fig. 13 shows the variations in diffusion loss with particle diameter of 30, 50, 75, 100, 150 and 200 nm of the charger at different aerosol flow rate of 0.3 and 1.5 L/min. Smaller particles were found to have a higher diffusion loss than larger particles due to the Brownian diffusion effect on particle motion in the charger. For each aerosol flow rate, the highest diffusion loss was seen to occur at particles with diameter of 30 nm to be about 62.50 and 19.33 % for the aerosol flow rate of 0.3 and 1.5 L/min, respectively. It was shown that high aerosol flow rate gave rise to minimum values of diffusion loss in the charger. Higher aerosol flow rate, hence, shorter residence time appeared to suppress the Brownian diffusion effect on particle motion in the charger. Fig. 14 shows the variations in electrostatic loss with particle diameter of 30, 50, 75, 100, 150 and 200 nm of the charger at different corona voltage of 2.3 – 2.9 kV and different aerosol flow rate of 0.3 and 1.5 L/min for positive and negative coronas. The highest electrostatic loss was observed to occur at particles with diameter of 75 and 50 nm to be about 86.29 and 72.92 % for positive and negative corona voltages of 2.9 and 2.5 kV, respectively. This was because the charged fraction of particles less than 75 nm in diameter decreased with decreasing particle diameter, while the electrical mobility of particle larger than 75 nm decreased as the particle size increased [9]. When the aerosol flow rate

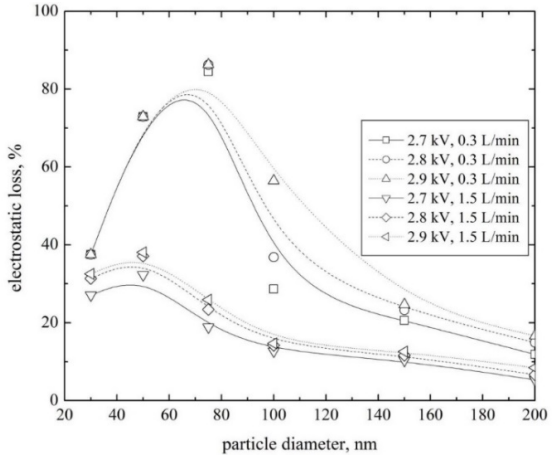

(a) Positive corona

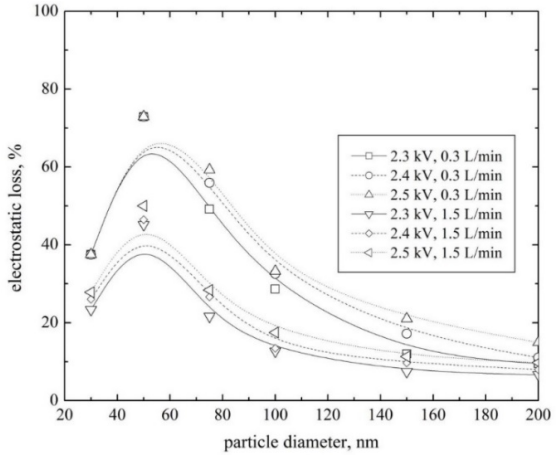

(b) Negative corona

Fig. 14 Variations in electrostatic loss with particle diameter of the charger at different corona voltage and aerosol flow rate for positive and negative coronas

increased, the electrostatic loss inside the charger was found to decrease. This was because the charged particles can to be transported from the charger more easily by the faster flowing aerosol.

4. Conclusion

In this paper, a unipolar corona-needle charger was designed as well as numerically and experimentally investigated to determine the corona discharges and particle losses in the charger at different corona voltages, aerosol flow rates and particle diameters for positive and negative coronas. Using a commercial computational fluid dynamics software package, COMSOL Multiphysics™, the electric field and charge distribution and the charged particle transport behaviors inside the charger were predicted. It was shown that the highest discharge currents of the charger were 9.835×10^{-6} A for positive corona, and 1.023×10^{-4} A for negative corona. The highest ion number concentrations in the discharge zone of the charger were found to be 1.087×10^{15} ions/m^3 for a positive corona voltage of about 3.2 kV, and 1.247×10^{16} ions/m^3 for a negative corona voltage of about 2.9 kV, and the highest $N_i t$ product for positive and negative coronas was found to be about 7.53×10^{13} and 8.65×10^{14} ions/m^3 s and occurred at the positive and negative corona voltages of about 3.2 and 2.9 kV, respectively, at the flow rate of 0.3 L/min. The highest diffusion loss was found to occur at particles with diameter of 30 nm to be about 62.50 and 19.33 % for the aerosol flow rate of 0.3 and 1.5 L/min, respectively, and the highest electrostatic loss was found to occur at particles with diameter of 75 and 50 nm to be about 86.29 and 72.92 % for positive and negative corona voltages of about 2.9 and 2.5 kV, respectively. Numerical simulation results of the electric field distribution and the charged particle migration inside the charger; showed good agreement with experimental results of the corona discharges and particle losses and can be used to support further improve, modify and refine the unipolar corona-needle charger. These results can be used as the proper operating conditions for the charger. The present charger proved to be particularly useful as an aerosol particle charger for positive and negative charges, used before the Faraday cup electrometer in an electrical aerosol detector.

Acknowledgements

The authors gratefully acknowledge the National Science and Technology Development Agency (NSTDA) (Research contract no. P-14-50757), the Thailand Research Fund (under the TRF contract No. RTA5980009) and the Nation Research University Project of Thailand Office of Higher Education Commission for the financial support. The authors wish to thank Dr. Rainer Zawadzki of Governor State University and Asst. Prof. Dr. Achariya Suriyawong, Department of Environmental Engineering, Faculty of Engineering, Chulalongkorn University for the valuable contribution during the preparation of the manuscript.

References

[1] J. Chang, A.J. Kelly, and J.M. Crowley, *Handbook of Electrostatic Processes*, Marcel Dekker, Inc., New York (1995).

[2] K.R. Parker, *Applied Electrostatic Precipitation*, Blackie Academic & Professional, New York (1997).

[3] P. Intra and N. Tippayawong, "An overview of unipolar charger developments for nanoparticle charging", *Aerosol and Air Quality Research*, vol. 11, no.2, pp. 186-208, 2011.

[4] P. Intra and N. Tippayawong, "Progress in unipolar

corona discharger designs for airborne particle charging: a literature review", *Journal of Electrostatics,* vol. 67, no. 4, pp. 605-615, 2009.
[5] K. T. Whitby, "Generator for producing high concentration of small ions", *Review of Scientific Instruments*, vol. 32, no. 12, pp. 1351-1355, 1961.
[6] A. Medved, F. Dorman, S. L. Kaufman, and A. Pocher, "A new corona-based charger for aerosol particles", *Journal of Aerosol Science,* vol. 31, pp. s616-s617, 2000.
[7] A. Marquard, M. Kasper, J. Meyer, and G. Kasper, "Nanoparticle charging efficiencies and related charging conditions in a wire-tube ESP at DC energization", *Journal of Electrostatics*, vol. 63, pp. 693-698, 2005.
[8] A. Hernandez-Sierra, F. J. Alguacil, and M. Alonso, "Unipolar charging of nanometer aerosol particle in a corona ionizer", *Journal of Aerosol Science*, vol. 34 pp. 733-745, 2003.
[9] M. Alonso, M. I. Martin, and F. J. Alguacil, "The measurement of charging efficiencies and losses of aerosol nanoparticles in a corona charger", *Journal of Electrostatics*, vol. 64, pp. 203-214, 2006.
[10] D. Park, M. An and J. Hwang, "Development and performance test of a unipolar diffusion charger for real-time measurements of submicron aerosol particles having a log-normal size distribution", *Journal of Aerosol Science*, vol. 38, no. 4, 420-430, 2007.
[11] C.L. Chien, C.J. Tsai, H.L. Chen, G.Y. Lin, and J.S. Wu, "Modeling and validation of nanoparticle charging efficiency of a single-wire corona unipolar charger", *Aerosol Science and Technology*, vol. 45, pp. 1468-1479, 2011.
[12] A. Marquard, J. Meyer, and G. Kasper, "Characterization of unipolar electrical aerosol chargers — Part II: Application of comparison criteria to various types of nanoaerosol charging devices", *Journal of Aerosol Science*, vol. 37, pp. 1069-1080, 2006.
[13] C. Qi, D. R. Chen, and P. Greenberg, "Performance study of a unipolar aerosol mini-charger for a personal nanoparticle sizer", *Journal of Aerosol Science*, vol. 39 450-459, 2008.
[14] P. Intra and N. Tippayawong, "Effect of needle cone angle and air flow rate on electrostatic discharge characteristics of a corona-needle ionizer". *Journal of Electrostatics*, vol. 68, no. 3, pp. 254-260, 2010.
[15] P. Intra and N. Tippayawong, "Design and evaluation of a high concentration, high penetration unipolar corona ionizer for electrostatic discharge and aerosol charging", *Journal of Electrical Engineering and Technology*, vol. 8, no. 5, pp. 1175-1181, 2013.
[16] COMSOL Inc., COMSOL Multi Physics Modelling Guide, Version 3.5a (2008).
[17] H. J. White, Industrial Electrostatic Precipitation, Addison-Wesley, Reading, Massachusetts (1963).
[18] W. C. Hinds, Aerosol Technology, John Wiley & Sons, New York, USA, 1999.
[19] G. P. Reischl, J.M. Makela, R. Harch, and J. Necid, "Bipolar charging of ultrafine particles in the size range below 10 nm", *Journal of Aerosol Science*, vol. 27, no. 6, pp. 931-939, 1996.
[20] C. J. Tsai, G. Y. Lin, H. L. Chen, C. H. Hunag, and M. Alonso, "Enhancement of extrinsic charging efficiency of a nanoparticle charger with multiple discharging wires", *Aerosol Science Technology*, vol. 44, pp. 807-816, 2010.

Panich Intra He received the BS. Tech. Ed. degree in Electrical Engineering from Rajamangala University of Technology Lanna, Thailand in 2001, the M.Eng. in Energy Engineering and Ph.D. degree in Mechanical Engineering from Chiang Mai University, Thailand in 2003 and 2006, respectively. He is currently an Associate Professor in the College of Integrated Science and Technology, Rajamangala University of Technology Lanna, Thailand.

Artit Yawootti He received BS. Tech. Ed. and M.Eng. degree in Electrical Engineering from King Mongkut's University of Technology Thonburi, Thailand in 2000 and 2006, respectively. He is currently a doctoral student in Energy Engineering at Chiang Mai University, Thailand.

Phadungsak Rattanadecho He received B. Eng. in Mechanical Engineering from King Mongkut's University of Technology Thonburi, Thailand in 1991, the M. Eng. in Mechanical Engineering from Chulalongkorn University in 1994, and the Ph.D. in Mechanical Engineering, Nagaoka University of Technology, Japan, 2002. He is currently a Professor in the Department of Mechanical Engineering, Thammasat University.